



Grey-Fuzzy Hybrid Optimization and Cascade Neural Network Modelling in Hard Turning of AISI D2 Steel

Ramanuj Kumar^{1*}, Anish Pandey¹, Amlana Panda¹, Rajshree Mallick¹, Ashok Kumar Sahoo¹

¹School of Mechanical Engineering,
KIIT Deemed to be university, Bhubaneswar, Odisha, INDIA -751024

*Corresponding Author

DOI: <https://doi.org/10.30880/ijie.2021.13.04.018>

Received 27 March 2020; Accepted 25 September 2020; Available online 30 April 2021

Abstract: Nowadays hard turning is noticed to be the most dominating machining activity especially for difficult to cut metallic alloys. Attributes of dry hard turning are highly influenced by the amount of heat generation during cutting. Some major challenges are rapid tool wear, lower tool-life span, and poor surface finish but simultaneously generated heat is enough to provide thermal softening of hard work material and facilitates easier shear deformation thus easy cutting. Also, plenty of works reported the utilization of various cooling methods as well as coolants which successfully retard the intensity of cutting heat but this leads to additional cost as well as environmental and health issues. However, still, there is scope to select proper cutting tool materials, its geometry, and appropriate values of cutting parameters to get favorable machining outcomes under dry hard turning and avoid the cooling cost, environmental, and health issue. Considering these challenges, current work utilizes PVD-coated (TiAlN) carbide insert in dry hard turning of AISI D2 steel. The multi-responses like tool-flank wear, chip morphology, and chip reduction coefficient are considered. The amalgamation of input processing variables must be optimum for the effectual performance of hard to process materials turning. Generally, the Fuzzy logic hypothesis represents the uncertainties co-related with fuzziness, and deficiency in the data concerned with the problem. Further, to achieve the best combination of input cutting terms, grey-fuzzy hybrid optimization (Type I and Type II) is utilized considering the Gaussian membership function. Type II grey-fuzzy system attributed to 15 % less error (between GRG and GFG) compared to Type I. Hence, Type II grey-fuzzy system is utilized to get the optimal set of input terms. The optimal combination of input terms is found as t-1 (0.15 mm), s-4 (0.25 mm/rev) and is Vc-2 (100 m/min) which is comparable to the results obtained under spray impingement cooling using CVD tool in the literature. However, hard turning can be assessed under the dry condition with a PVD tool at the obtained optimal input condition for industrial uses. Further, six different types of cascade-forward-back propagation neural network modelling is accomplished. Among all models, CFBNN-4 model exhibited the best prediction results with a mean absolute error of 2.278% for flank wear (VBc) and 0.112% for the chip reduction coefficient (CRC). However, this model can be recommended for other engineering modelling problems. The outcomes of this research may be of immense importance to the tool manufacturers and machining industry.

Keywords: Hard turning, optimization, grey-fuzzy, cascade neural network, flank wear, chip reduction coefficient, ANOVA

1. Introduction

Hardened D2 steel (above 55 HRC) stands under extremely hard material and it comes under difficult to cut category since the conventional machining process experienced lots of challenges [1]. The major challenges under dry cutting of hardened steel are the higher tool wear, poor quality of finish, higher cutting forces, higher specific energy

consumption, etc. which leads to higher tooling cost thus costlier machining. But simultaneously, dry machining is very favorable because of the generation of sufficient amount heat which attributed the thermal softening of hard work material and facilitates easier shear deformation thus cutting phenomena easier [2].

Turning of hardened steel (> 45 HRC) is called as hard turning [3-4]. Earlier days, grinding process is commonly implemented to machine hardened steel but since recent years, hard turning process successfully swapped the grinding process due to numerous benefits like lesser energy utilization, relatively very higher metal removal rate, lower machining expenditure per piece, flexible for interrupt machining, relatively low tool inventory, no need of coolant thus disposal and maintained of coolant not required. Also, the hazardous issue is completely avoided through dry cutting. In recent years, near dry machining becoming popular but it leads to extra cost. Thus, there is always scope to select proper cutting tool and tool geometry to get the favorable requirements of machining and avoid the cooling and lubrication cost in machining. Since three decades, various cutting tools like CBN, PCBN, PVD coated carbide, CVD coated carbide, ceramic, cermet, and uncoated carbide were implemented in hard machining concern [5-6]. The CBN and PCBN tools were exceedingly utilized in hard metal machining due to their high resistance ability against abrasive wear, chemical diffusion wear [7]. The ceramic tool attributed the extensive tool life and reduced cutting forces relative to PCBN tool and tool failure occurred due to the dominance of abrasion, diffusion and adhesion phenomena during AISI D2 machining [8]. The PCBN tool can be preferable over carbide tool due to its delayed wear growth in turning of D2 steel [9]. The cutting temperature noticed to be a key factor towards rapid tool wear of PCBN tool and it was leading due to rise in cutting speed and feed but cutting speed was more dominant than feed [10]. Abrasion and grooving mode of wears were identified as the main tool failure mechanisms. An abrasion phenomenon was more dominant due to the hard elements associated with D2 steel [11]. Saw tooth pattern on the edge of chips in orthogonal machining of AISI D2 hard steel was traced due to crack propagation of quenched structure of material. Also, chips became soft and ductile at elevated speed machining which attributed the chip segmentation and look like saw tooth design on chips [12]. During machining, a tribo-film at friction surfaces induced that directly influenced the tool life of ceramic insert in hard machining of D2 steel [13]. The wiper geometry of ceramic cutting insert attributed the superior quality surface compared to conventional geometry insert [14-15]. The machined surface quality was impressively dominated by depth of cut, followed by longitudinal feed and cutting speed [16-17]. TiC coated tool had the higher wear resistance capability compared to TiN coated during the turning of D2 and D3 steel [18]. The smooth growth in the wear of coated tools compared to the uncoated and wearing region was localized on to tool-nose [19]. The effects of cutting heat on to the finish surface integrity, tool-life and dimensional precision in machining on AISI 4340 steel with PVD and CVD coating cutting tool was studied. Speedy wear followed by catastrophic tool-breakage was foremost for the PVD tool while the gradual development of wear was perceived for the CVD tool [20-21].

Some of the researchers have evaluated the machining performance of hardened steel. Panda et al. [22] contributed the modeling and optimization of cutting force, surface roughness, and tool wear during hard turning of D3 steel with mixed ceramic tool. The response surface methodology followed by genetic algorithm and particle swarm optimization have been used for multiple response output optimizations. Panda et al. [23] performed machining performance, development of mathematical models, multiple-output response parametric optimization, computation of life of the cutting tool, through cutting of AISI 4340 hardened steel under dry environment using TiN coated mixed ceramic inserts. Panda et al. [24] performed machining performance, development of mathematical models, multiple-output response parametric optimization, computation of life of the cutting tool, through cutting of AISI 4340 hardened steel under dry environment using TiN coated mixed ceramic inserts. Das et al. [25] performed hard part turning process using untreated and cryo treated cermet inserts under dry machining situation. It was suggested that tempered uncoated deep cryo treated cermet cutting tool outperformed enhance results in comparison to other type of cermet inserts. Anand et al. [26] performed the review analysis on machining and performance characteristics for improvement of hardened steels during hard part turning applicable in mold, die making, and die making enterprises.

Selection of optimal dry turning, parameters is greatly imperative to get a lower wear rate and good quality of finish. Numerous optimization techniques have been used in hard turning problems to obtain the optimal set of cutting parameters. Conventional multi-attributes optimization methods like Grey, TOPSIS, WPCA, etc. and soft computing optimization techniques like particle swam, fuzzy, ANN, etc. were utilized in dry turning. Nowadays, researchers are giving more emphasis on hybrid or mixed optimization approach that comprises of conventional and soft computing techniques. Grey-Fuzzy the concept was found to be a fast and efficacious technique in the field of machining [28]. According to Suresh et al. [29], the grey-fuzzy algorithm offered an improved grey-fuzzy-grade with minimal deviation in output compared to the grey technique. Hong and Chiang [27] utilized the Grey-Fuzzy concept to the optimization of the turning process and found a great enhancement in the requisite performance index. Krishnamoorthy et al. [30] accomplished the drilling operation using grey-fuzzy techniques and the obtained results proposed that the quality of produced holes was importantly improved. Das et al. [31] also found a significant gain in grey-fuzzy grade compared to grey relational grade hence it was purposed the grey-fuzzy concept will be efficaciously utilized for the optimization problem.

In the past research study, it was found that the dry hard cutting condition is mostly carried using CBN, PCBN, Ceramic, coated carbide (CVD), uncoated carbide inserts. Rarely investigation reported the application of PVD-coated carbide insert in hard turning of AISI D2 steel. In addition, the application of coolant and its delivery instruments

attributed the additional cost in total machining cost. However, dry cutting technology needs to be more elaborated to meet the industrial requirement of low budget machining. Furthermore, implementation of grey-fuzzy based hybrid approach with aforesaid cutting conditions is rarely performed. In light of the foregoing reasons and to get the desired optimal setting for cutting input parameters, a grey-fuzzy-based hybrid approach found to be a more efficient tool, hence it is utilized in the current work to get the best combination of input terms. Keeping this in view, a careful experimental investigation and optimization is therefore necessitated.

In the current paper the research gap has been identified followed by the objectives regarding to the related literature review. Further, the next section is described with materials and methods in section 2. The machinability indicators are tool flank wear, chip reduction coefficient and microphotography of chips. On the basis of experimentation performed the results and discussions are illustrated in section 3. The grey fuzzy optimization approach is provided in section 4. Furthermore section 5 is described regarding cascade ANN modeling. At last, the conclusions of this research work and future outlook are delineated in Section 6.

2. Materials and Methods

The current hard turning experiments are accomplished considering L16 Taguchi design where the number of the input variables is 3 and their levels are 4. The input terms are depth of cut (t (mm) = 0.15, 0.25, 0.35 and 0.45), feed (s (mm/rev) = 0.1, 0.15, 0.20 and 0.25) and cutting speed (v_c (m/min) = 50, 100, 150 and 200). Hardened AISI D2 steel bar (ϕ 45mm x L175 mm) of hardness 55 HRC is chosen for the investigation due to its diverse application in the automobile sector, tooling industries, etc. JYOTI make DX 200 4A CNC Lathe is utilized for the turning experiments. The cutting range of input parameters were finalized on the basis of trial runs, experience, and knowledge found in extensive literature review relating to hard part turning and cutting tool manufacturer's catalogue [32]. PVD applied TiAlN cemented carbide (CNMG 120408) insert with a rhombus shape with an 80° angle and 0.8 mm nose radius supplied by WIDIA is used for the experimentation. PCLNR2525 insert holder is utilized to screw the inserts. The new edge of the insert is used for each experiment. Flank wear (VBc), chip morphology and chip reduction coefficient (CRC) are studied with the help of images drawn by Olympus to make optical microscope and chip thickness measured through the digital caliper. MINITAB 17 is utilized for ANOVA and main effects plot while MATLAB R2013a is utilized for grey-fuzzy hybrid optimization of the cutting responses. Graphical presentation of entire work is displayed in Fig.1.

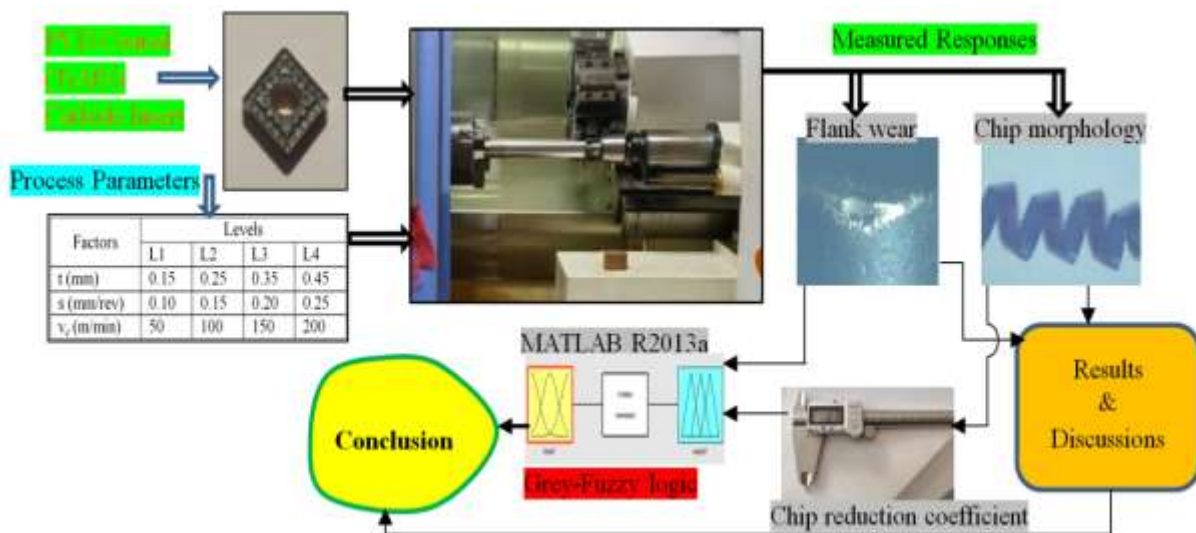


Fig. 1 - Graphical presentation of entire work

3. Results and Discussions

The L_{16} [33] set of turning parameters, flank wear (VBc), chip reduction coefficient (CRC) and chip morphology results are located in the Table 1.

Table 1 - Measured results data

Test No.	t mm	s mm/rev	v _c m/min	VBc mm	CRC = a _z /Sinφ	Chip morphology	
						Shape	Colour
1	0.15	0.1	50	0.020	1.907	Helical	Metallic
2	0.15	0.15	100	0.023	1.806	Helical	Metallic
3	0.15	0.2	150	0.028	1.656	Helical	Metallic
4	0.15	0.25	200	0.052	1.525	Broken 'c' and 'e' type	Blue
5	0.25	0.1	100	0.024	2.042	Helical	Metallic
6	0.25	0.15	50	0.026	1.873	Helical	Metallic
7	0.25	0.2	200	0.061	1.706	Helical	Blue
8	0.25	0.25	150	0.037	1.606	Helical	Metallic
9	0.35	0.1	150	0.064	2.062	Helical	Metallic
10	0.35	0.15	200	0.093	1.862	Broken c type	Blue
11	0.35	0.2	50	0.028	1.957	Broken 'c' and 'e' type	Metallic
12	0.35	0.25	100	0.030	1.806	Broken 'c' type	Metallic
13	0.45	0.1	200	0.161	2.000	Broken 'c' type	Blue
14	0.45	0.15	150	0.083	1.940	Helical	Blue
15	0.45	0.2	100	0.030	1.932	Broken 'c' type	Metallic
16	0.45	0.25	50	0.038	1.967	Broken 'c' type	Metallic

3.1 Wear Analysis

When the coating is gradually removed from the cutting insert, the tool tips still collapse within a few times when the coating is removed. As a result, understanding the mechanisms in relation with tool wear is vital to enhance the machining responses in the most of the challenging issues in the industrial applications. In hard turning process, an observable fact of tool flank wear is on cutting tool flank face. Tool flank wear has important significance in the hard part turning and is considered as life of the tool criteria. The flank wear is impacted by cutting tool geometry, machining parameters, and Flank wear is influenced by tool geometry, cutting parameters, and work piece-tool characteristics. The harder work surface can result in the additional serious abrasive wear on the flank face of the cutting tool. In general, built up Edge (BUE) caused by the adhesive wear mechanism happened on the cutting tools under all machining conditions [34]. Cutting temperature at the tool work interface zone is increased due to accelerated cutting speed. Therefore, due to enhancement of cutting speed, chemical wear becomes a prominent wear pattern accelerating weakening the tool tip resulting in tip breakage (chipping) [35]. In today's competitive scenario, industries are very much concerned about tooling cost and it should be low. Tooling cost depends on the number of work piece machined by a single tip of the tool. However, tool tip wear analysis is essential in hard turning. In the current work, tool-flank wear is analyzed based on the worldwide acceptable limit of wear width (VBc) = 0.3 mm [36].

Wear results as shown in Table 1 are identified under the limit of 0.3 mm i.e. the selected tool and input parameters ranges are well acceptable for hard turning purpose. The obtained results are also comparable with results obtained in spray cooling condition by CVD tool [28] and the results obtained by ceramic tool under dry scenario [5]. Graphical plot (Fig. 2) confirms that the tool-flank wear increasing with depth of cut while beyond 100 m/min of cutting speed, wear width steeply elevating whereas up to 0.2 mm of feed, wear width reduces sharply and beyond it, wear width increases. Numerically, for each depth of cut, wear width is increasing with the cutting speed (v_c) i.e. the cutting speed is the most foremost term towards tool-flank wear and it is confirmed by ANOVA (Table 2) report as the impact of cutting speed on VBc was topmost (54.06 %). Similar findings were noticed by several researchers [37-38]. The ANOVA analysis is performed at a confidence level of 95% (i.e.5% significance level) [39]. Impact of depth of cut (26.04 %) is also considered because of the generation of higher radial force during cutting while the negative effect of feed on VBc (almost sharp decrement in VBc with leading feed) confirms that the PVD tool can be suitable to machine the hard work piece at higher feed rate.

The Tool-wear mechanism is highly essential to understand the tool failure mechanism. Abrasion, micro-chipping, chipping, sever chipping (tool-tip lost) and built-up edge are the mechanism identified on the tool tip as shown in Fig. 3. Several works reported that the abrasion is most dominating in nature during machining of hard materials due to continuous interaction of the continuous chips (contain hard elements) with a tool-flank face [40]. Further, as hot continuous chips is interact with the smooth and clean surfaces of tool tip, a bond between chip-tool develops called as built-up edge (BUE) as noticed in run 11 (Fig. 3(c)). Further, with the progress of machining, this BUE removed along with parent layer of tool as result micro-chipping and chipping phenomena attributed on to the tool tip as shown in Fig. 3f-h. This micro-chipping/chipping makes the cutting-edge interrupt which affects the surface quality. Also, elevated cutting temperature at highest speed cutting condition (200 m/min) attributed the sever chipping or some instant tool-tip gets lost as shown in Fig. 3(h).

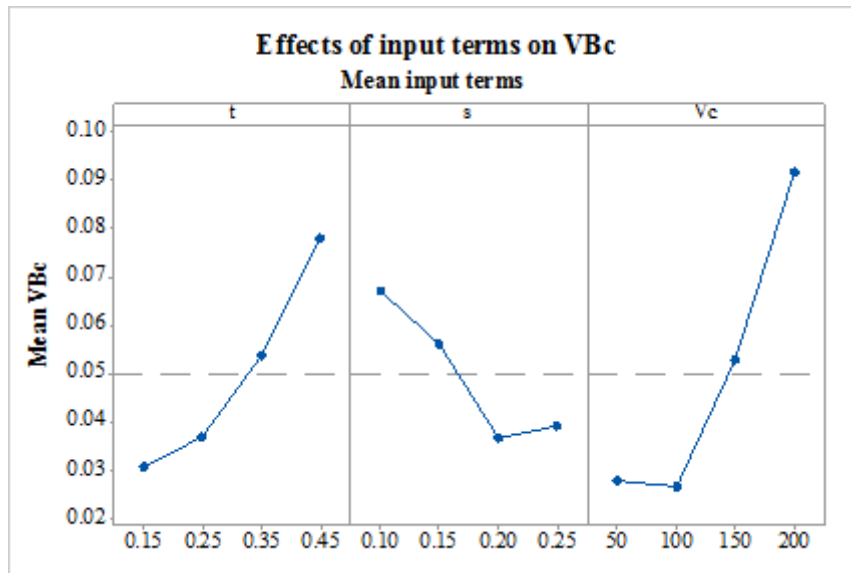


Fig. 2 - Graphical representations of effects of input terms on flank wear (VBc)

Table 2 - Estimation of impact of input terms on VBc by ANOVA

Basis	DF	Seq SS	Adj MS	F	P	% impact	Comments
t	3	0.005350	0.001738	6.80	0.023	26.04	Significant
s	3	0.002510	0.000836	3.19	0.105	12.22	Insignificant
v _c	3	0.011106	0.003702	14.11	0.004	54.06	Significant
Inaccuracy	6	0.001574	0.000262				
Aggregate	15	0.020541					

S = 0.0161993 R-Sq = 92.34% R-Sq(adj) = 80.84%

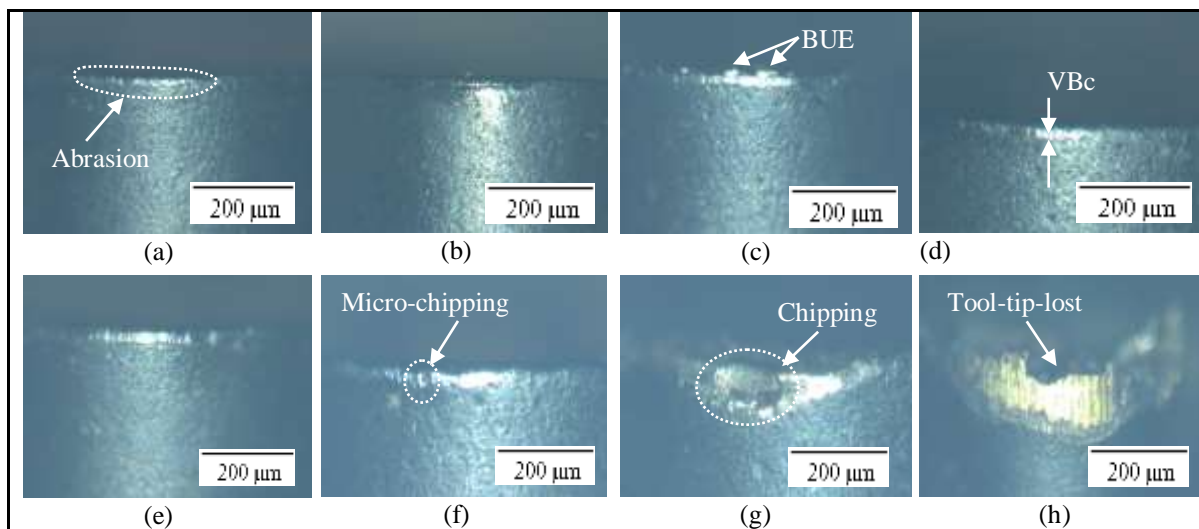


Fig. 3 - Flank wear micrographs a-d) lowest v_c (runs 1, 6, 11, and 16) = 50 m/min e-h) highest v_c (runs 4, 7, 10 and 13) = 200 m/min

3.2 Chip Reduction Coefficient and Chip Pattern Analysis

Chip reduction coefficient (CRC) usually indicates the machinability behavior, either it is favorable or not [41]. The measurement of chip reduction coefficient (ζ) is an important performance criterion, since it explains machining characteristics like favorable or unfavorable machining regarding specific consumption. Moreover, it is the extent of plastic deformation in cutting action [42] depth of cut increased to 0.35 mm beyond it CRC increases with a relatively slower rate. Further, while increasing feed from 0.1 to 0.25 mm/rev, CRC drastically decreases and similarly variation in CRC is noticed with leading speed but decrement rate of CRC was lower than feed which is confirmed through

impact analysis through ANOVA (Table 3), as the impact of feed (43.11 %) on CRC is about 2.54 times more than cutting speed (15.92%). Singh et al. [43], also found a decrement in CRC with leading feed. ANOVA also reported that all the input terms significantly influence the CRC.

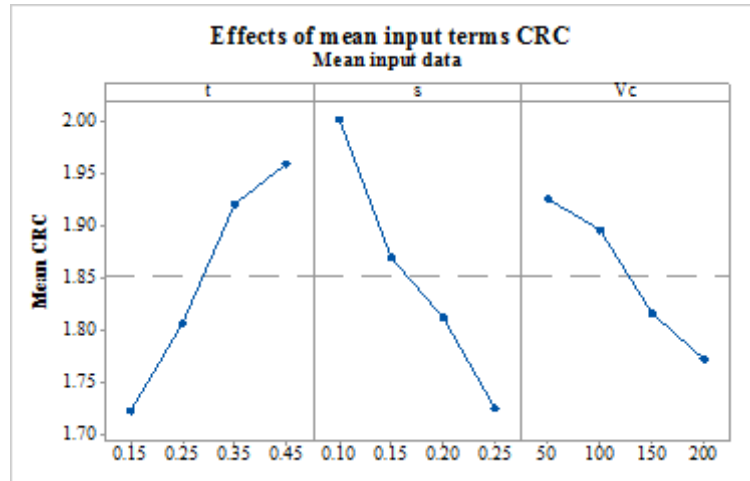


Fig. 4 - Graphical representations of effects of input terms on chip reduction coefficient

Table 3 - Estimation of impact of input terms on CRC through ANOVA

Basis	DF	Seq SS	Adj MS	F	P	% impact	Comments
t	3	0.14013	0.04671	20.54	0.001	37.32	Significant
s	3	0.16189	0.05396	23.73	0.001	43.11	Significant
v _c	3	0.05980	0.01993	08.77	0.013	15.92	Significant
Inaccuracy	6	0.01365	0.00227				
Aggregate	15	0.37546					

S = 0.0476889 R-Sq = 96.37% R-Sq(adj) = 90.91%

During the current cutting action, each chip has possessed wavy shaped pattern (also called as saw tooth or segmented chips) on its edge as shown in Fig. 5. Similar observation noticed by Kumar et al., [6] under dry cutting. Initially, when the edge of the tool comes in contact with work piece, the closer to tool portion of material gets compressed due to high cutting pressure while the subsequent work portion is getting bulge. Further with the progress of cutting, this bulge portion tends to slip towards the free surface and takes a shape of the saw tooth. During this cutting phenomenon, plastic deformation of work is transformed into heat thus thermal softening of work-material occurs in the primarily deformed section. Further with repetition of cycles attributed the saw tooth formation or chip segmentation. This segmentation significantly influences the chip cross-section thus; cutting forces fluctuates [41]. Chip pattern is considerably affected by level of input terms combination, with least depth of cut (0.15 mm) and till moderate speed and feed (up to 150 m/min of speed and up to 0.20 mm/rev of feed) chip pattern is of helical type with metallic colour which ensures the favorable machining and it is confirmed by VBc values (0.02 mm to 0.028 mm) while at highest feed and speed (run 4), broken chips (discontinuous chips) with ‘c’ and ‘e’ in shape with blue colour chips produced which significantly influenced the machining performance and it is confirmed as relatively higher VBc value (0.052 mm) is achieved at this condition. Similarly, in other test runs, broken chips (runs 10, 12, 13 and 15) are noticed with moderate to largest feed (0.1 to 0.35 mm/rev) and highest cutting speed (150 to 200 m/min) conditions. In run 11 and run 16, although the speed is least (50 m/min) feed values are higher (0.2 and 0.25 mm/rev) which attributed the broken chips formation. Helical pattern chips (Fig. 5 and Table 1) attributed the favorable machining. Blue colour chips denoted the higher heat generation compared to other machining tests where metallic chips produced. Similar illustration reported by [43].

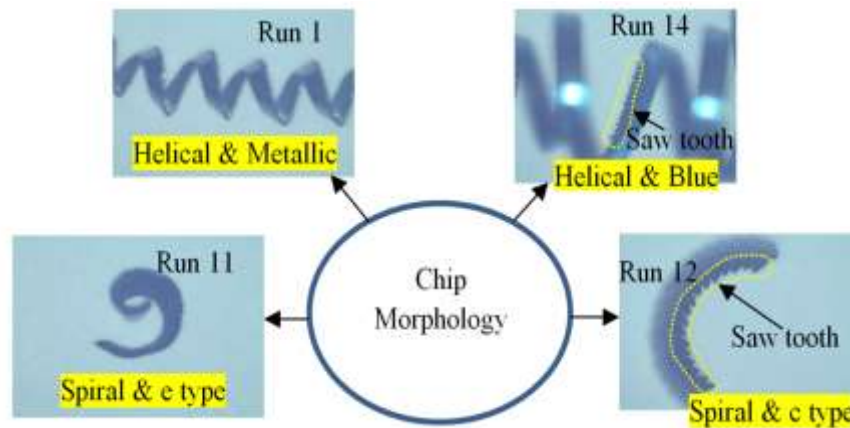


Fig. 5. Different patterns of chips

4. Grey-fuzzy Optimization

The fuzzy system provides an enhanced GRG which confirms the lesser uncertainty in output relative to the grey process. Due to this, nowadays the grey-fuzzy logic was popularly utilized in various engineering applications [44-45]. The details of grey and fuzzy system are as follows:

4.1 Grey Relational Analysis (GRA)

The Grey analysis's main objective is to optimize the data set's process parameters, developed by Professor Deng. Also, this analysis establishes a relationship between the desired and actual experimental data. In the present study, the Grey analysis gives the optimum level of inputs and outputs data, and according to these data, we minimize the various machine parameters. Moreover, this Grey analysis's main advantage is that it can provide more excellent optimum value in less dataset [46]. Grey concepts offer competent management on the discrete, uncertainty and multi-input data [30]. The GRA measures the absolute value of the data difference between sequences. It is also utilized to provide a close correlation among sequential data [24-25]. Many works were reported the effective utilization of GRA for analysing the co-relation among sequences for a smaller number of data [47-48].

The following steps were utilized to conduct the GRA analysis [49-50]:

Step-1 Normalize the flank wear and chip reduction coefficient experimentally measured data in the range of 0 to 1 taking lower is better concept. This process is called grey relational generation.

Step-2 Estimation of grey relational coefficient (GRC) for all the outputs.

Step-3 Estimation of grey relational grade (GRG) by taking the average of respective GRC.

Step-4 Estimation of mean GRG taking each factor with their levels.

Step-5 Selection of optimal levels of input cutting terms.

Step-6 Analyse experimentally measured output data using GRG and ANOVA

The equations to estimate the terms linked to Steps-1 to 3 are listed in Fig. 6 and the calculated data is listed in Table 4.

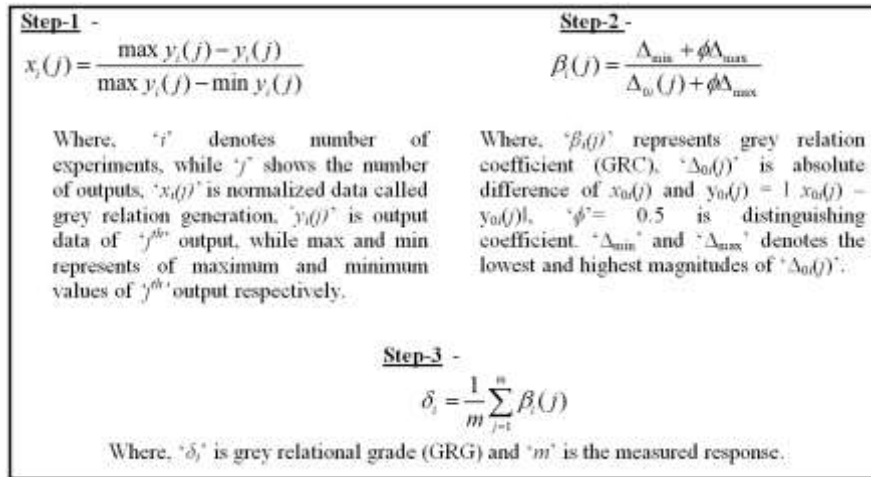


Fig. 6 - Steps to estimate the grey relational grade (GRG)

Table 4 - Estimation of grey relational grade (GRG)

No	Normalized value VBc	CRC	Grey relational coefficient GRC-VBc	GRC-CRC	Grey relational grade GRG	Rank
1	1	0.2886	1	0.4128	0.7064	5
2	0.9787	0.4767	0.9592	0.4886	0.7239	4
3	0.9433	0.7561	0.8981	0.6721	0.7851	3
4	0.7730	1	0.6878	1	0.8439	1
5	0.9716	0.0372	0.9463	0.3418	0.6441	8
6	0.9574	0.3520	0.9216	0.4355	0.6785	7
7	0.7092	0.6629	0.6323	0.5973	0.6148	11
8	0.8794	0.8492	0.8057	0.7682	0.7870	2
9	0.6879	0	0.6157	0.3333	0.4745	13
10	0.4823	0.3724	0.4913	0.4434	0.4674	14
11	0.9433	0.1955	0.8981	0.3833	0.6407	9
12	0.9291	0.4767	0.8758	0.4886	0.6822	6
13	0	0.1155	0.3333	0.3611	0.3472	16
14	0.5532	0.2272	0.5281	0.3928	0.4605	15
15	0.9291	0.2421	0.8758	0.3975	0.6366	10
16	0.8723	0.1769	0.7966	0.3779	0.5873	12

4.2 Fuzzy Logic

Grey theory works on three basic rules namely lower the better, nominal the better and higher the better. But still, some level of uncertainty is associated with the acquired results. This uncertainty can be efficaciously curbed through a fuzzy concept [44]. However, a fuzzy logic of multi-attributes was developed and popularly known as grey-fuzzy logic. The optimization function can be executed on a single response called a grey-fuzzy grade in spite of complex multi-responses.

The fuzzy system includes a fuzzifier, a membership function, rule inference, an inference engine, and a defuzzifier. In the initial step, fuzzifier utilize the membership function to fuzzify inputs (GRC-VBc = grey relation coefficient for flank wear, and GRC-CRC = grey relation coefficient for chip reduction coefficient) as mentioned in Table 4. Membership function defines the mapping of inputs (GRC-VBc and GRC-CRC) and output (GFG) in the range of 0 to 1. Matlab (R2013a) fuzzy tool box is utilized to get the grey-fuzzy-grade. In the literature, many type of membership functions like Gaussian, trapezoidal, sigmoidal, and triangular have been used. Among them Gaussian membership function is outperformed. However, the current work utilized the Gaussian membership function. Further, two types of grey-fuzzy logics are utilized based on number of membership function. In Type-I, membership function for inputs and output is same and equal to five [VL = very low, L = low, M = medium, H = high and VH = very high] while in Type-II, membership function for input is five [VL = very low, L = low, M = medium, H = high and VH = very high] and for output it is seven [VVL= very low, VL = very low, L = low, M = medium, H = high, VH = very high and VVH = very high]. The membership graph for input and output is displayed in Fig. 7 and Fig. 8 respectively. Type 1 consists of 13 distinguish rules and Type II carries 15 distinguish rules as mentioned in Table 5. Further, the

grey fuzzy grade data is defuzzified. Many defuzzification techniques namely centroid methods, weighted average method, mean-maximum membership method, and maximum-membership method were found in literature. Out of them, centroid techniques were most prevalent. However, current work uses centroid based defuzzification to get the crispy data [29]. Further, the rules viewer of test-4 for Type I and Type II are displayed through Fig. 9 and Fig. 10 consequently. In rule viewer figures (Fig. 9 and Fig. 10), rows denote the number of membership function rules, 1st and 2nd column represent input terms (i.e. GRC for experimental measured data of VBc and CRC) and 3rd column represent output i.e. defuzzified value in term of GFG (grey fuzzy grade).

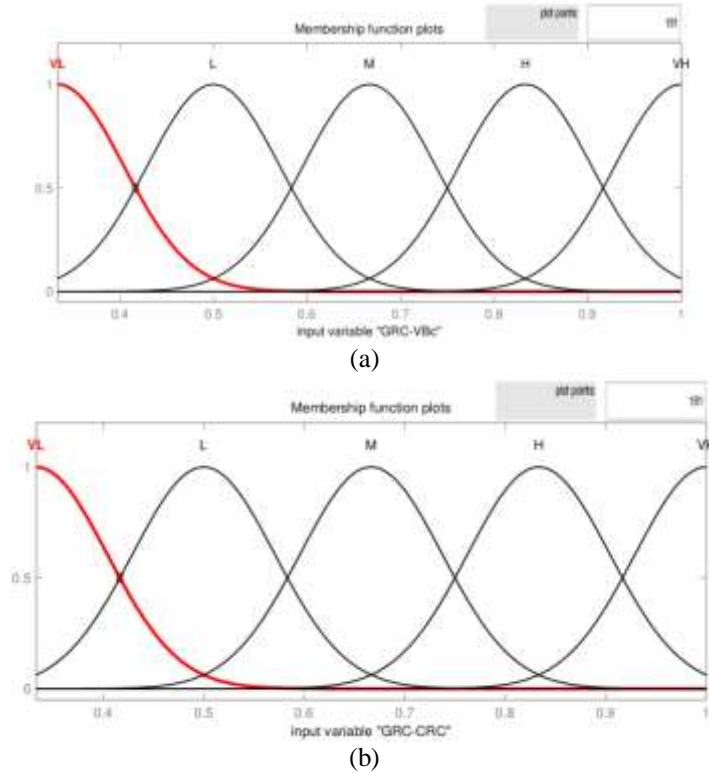


Fig.7 - Membership function graphs of Type I and Type II for inputs a) GRC-VBc and b) GRC-CRC

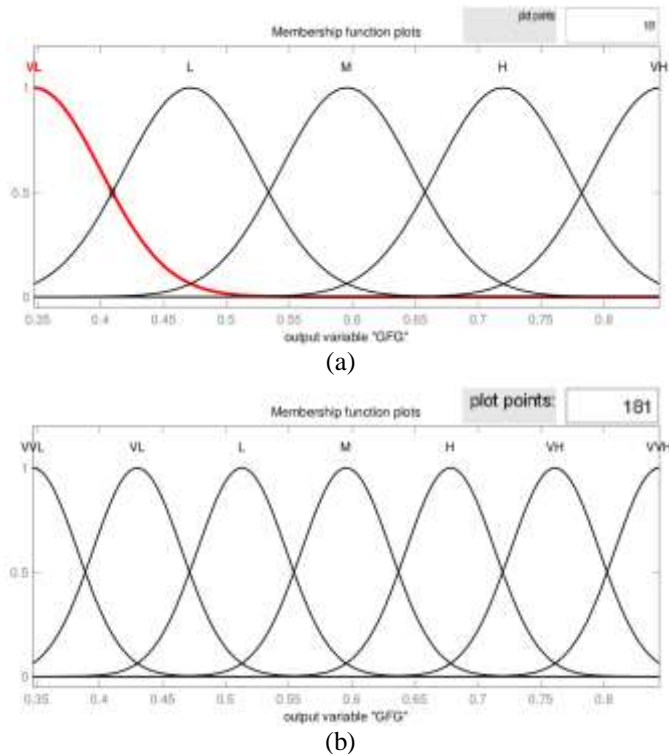


Fig. 8 - Membership function graphs of output grey-fuzzy grade (GFG) for (a) Type 1 (b) Type II

Table 5 - Membership functions for Type I and Type II fuzzy system

No.	Type-I			No.	Type-II		
	GRC-VBc	GRC-CRC	GFG		GRC-VBc	GRC-CRC	GFG
1	VH	L	H	1	VH	L	H
2	H	M	VH	2	VH	L	VH
3	M	VH	VH	3	H	M	VH
4	VH	VL	M	4	M	VH	VVH
5	VH	L	M	5	VH	VL	H
6	M	M	M	6	M	M	M
7	H	H	VH	7	H	H	VH
8	M	VL	M	8	M	VL	L
9	L	L	L	9	L	L	L
10	H	VL	M	10	H	VL	H
11	H	L	H	11	H	L	H
12	VL	VL	VL	12	VL	VL	VVL
13	L	VL	L	13	L	VL	VL
				14	H	VL	H
				15	H	VL	M

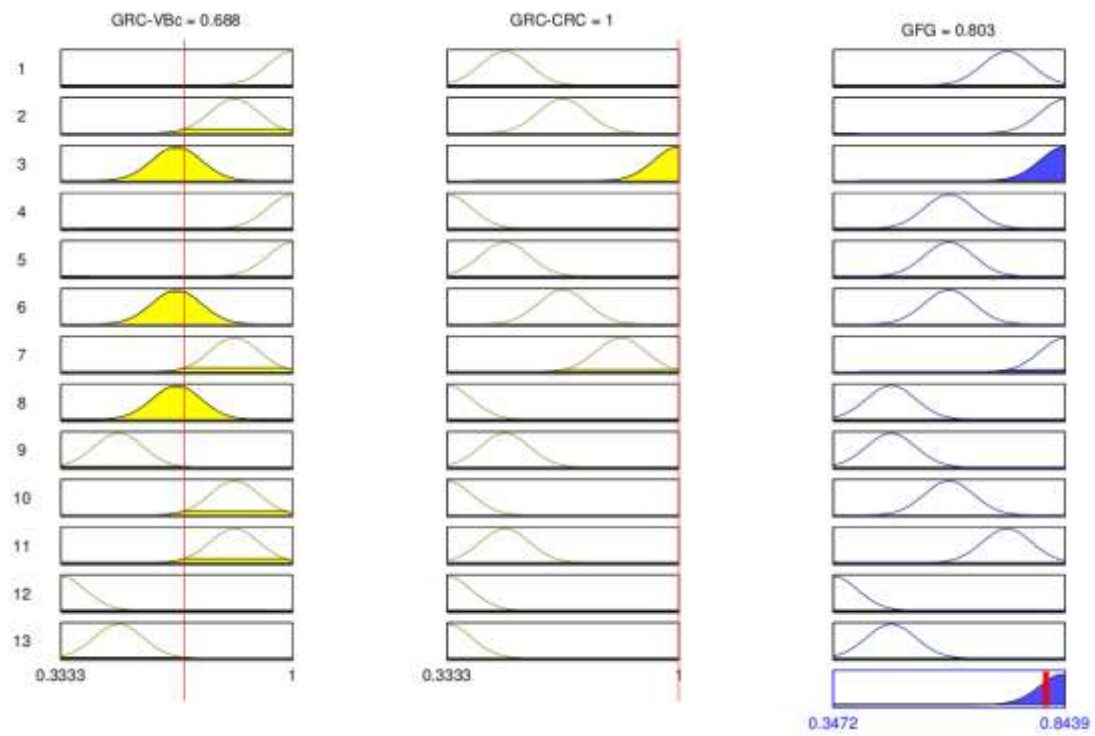


Fig. 9 - Fuzzy rules viewer of Type I (Exp. No. 4)

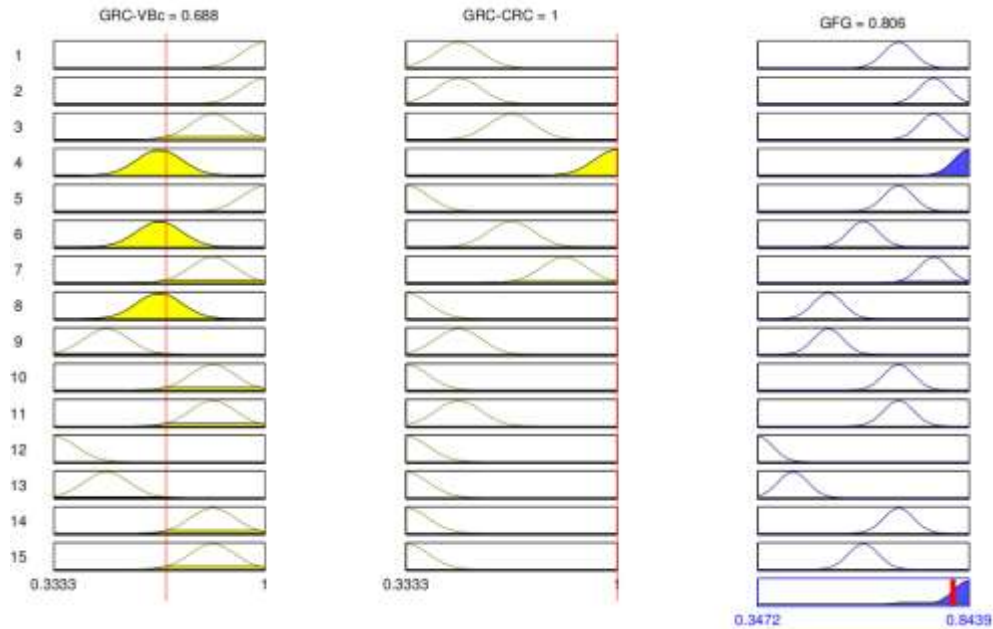


Fig. 10 - Fuzzy rules viewer of Type II (Exp. No. 4)

Further, with the help of rules viewer, the GFG data of all experiments for Type I and Type II are estimated and listed in Table 6. Also, the obtained data of GFG is compared with GRG and displayed graphically through Fig. 11. Further, the error (absolute) between GRG and GFG has been estimated using the Eq. 1 [51] and noted in Table 6. The mean absolute error between GRG and Type I-GFG is estimated at 4.731% while it is 4.016% for GRG and Type II-GFG. Type II GFG contains 15 % less error compared to Type I, hence to get the optimal condition, Type II GFG data has been taken.

$$Mean - absolute - error(MAE)\% = \frac{|(GRG - GFG)|}{GRG} 100 \tag{1}$$

Further, to estimate the optimal combination, mean GFG (Type II) is estimated for each factor and each level and displayed in Table 7. Higher mean value for level of each parameter represents the optimal level of input variables. However, the optimal parametric combination is found as t1-s4-vc2. Further, surface plots (Fig. 12) displayed the influence of input terms on GFG. Higher GFG is noticed at moderate VBc and higher CRC values. ANOVA (Table 8) was utilized to estimate the most contributing input factor for the GFG. From ANOVA (Table 8), depth of cut (t) contributed the highest (51.7%) followed by feed (26.57%) and speed (16.37%) on GFG. All the turning input terms are noticed to be noteworthy at 95% of confidence. Further, confirmatory results are obtained and found an improvement in GFG relative to GRG. Also, a gain in GFG from initial setting is noticed as located in Table 9. However, the current hybrid optimization technique can be a reliable choice towards industrial applications.

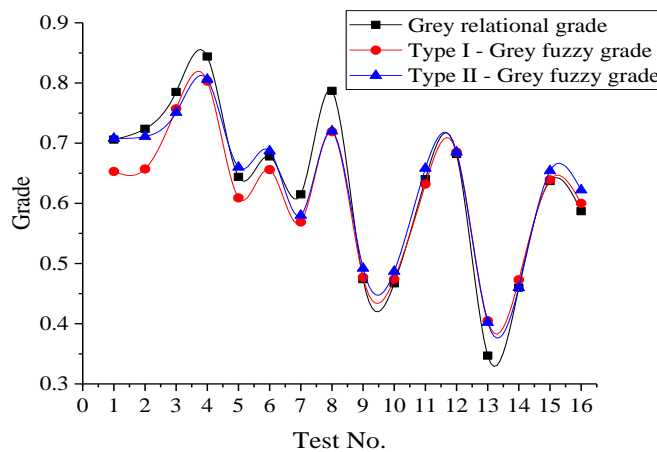


Fig. 11 - Comparative graphs between GRG and GFG

Table 6 - GFG data for Type I and Type II and absolute error between GRG and GFG

No.	Experimental (GRG)	Type 1 (GFG)	Absolute error (%)	Type 2 (GFG)	Absolute error (%)
1	0.706	0.653	7.557	0.708	0.229
2	0.724	0.657	9.242	0.711	1.783
3	0.785	0.757	3.578	0.751	4.342
4	0.844	0.803	4.847	0.806	4.491
5	0.644	0.609	5.444	0.660	2.474
6	0.678	0.656	3.323	0.687	1.246
7	0.615	0.569	7.451	0.580	5.662
8	0.787	0.719	8.638	0.720	8.511
9	0.474	0.477	0.521	0.492	3.682
10	0.467	0.474	1.420	0.487	4.202
11	0.640	0.632	1.357	0.658	2.701
12	0.682	0.685	0.410	0.685	0.410
13	0.347	0.405	16.637	0.402	15.773
14	0.460	0.473	2.723	0.460	0.100
15	0.637	0.639	0.372	0.654	2.728
16	0.587	0.600	2.170	0.622	5.916
Average absolute error			4.731	4.016	

Table 7 Mean GFG and optimal level of input terms

Inputs	Levels of input terms				$\Delta=(\max-\min)$	Rank	Optimal level
	L-I	L-II	L-III	L-IV			
t	0.744	0.662	0.581	0.535	0.209	I	1 st
s	0.566	0.586	0.661	0.708	0.142	II	4 th
v _c	0.669	0.678	0.606	0.569	0.109	II	2 nd

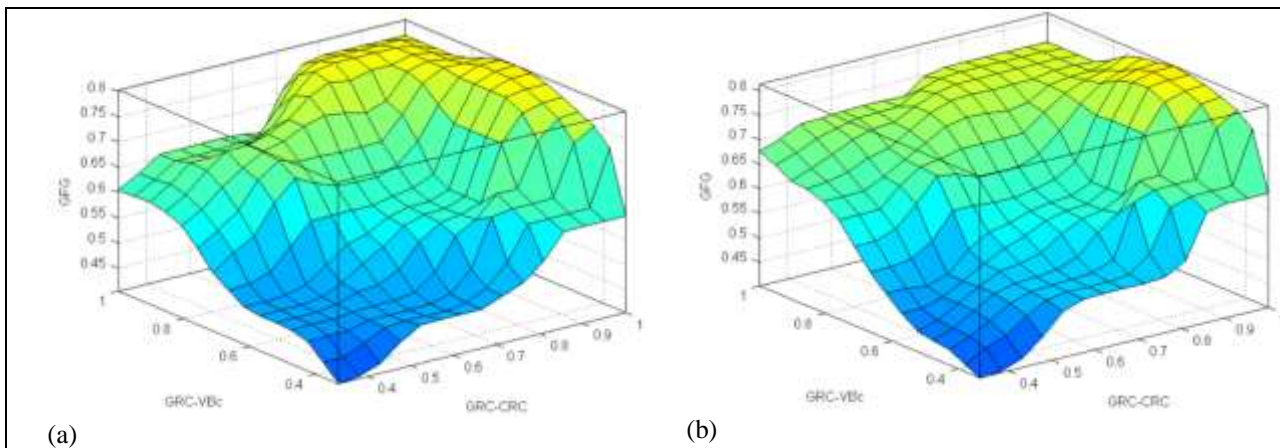


Fig. 12 - Effects of output response on Grey fuzzy grade (a) Grey-fuzzy Type I; (b) Grey-fuzzy Type II

Table 8 - Contribution of input terms on GFG by ANOVA

Terms	DF	Adj SS	Adj MS	F	P	Contribution (%)
t	3	0.10230	0.03409	19.34	0.002	51.70
s	3	0.05257	0.01752	9.94	0.010	26.57
v _c	3	0.03239	0.01079	6.12	0.029	16.37
Residuals	6	0.01058	0.00176			05.36
Total	15	0.19784				

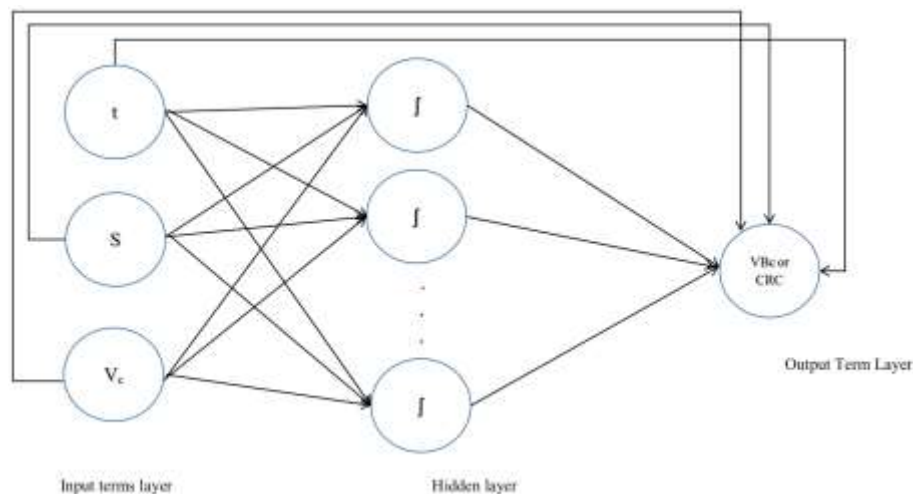
Table 9 - Optimal and predicted results

Setting terms	Initial turning parameters	Optimal turning parameters	
	t4-s1-v _c 4	Prediction	Experiments
VBc	0.093		0.024
CRC	1.862		1.656
GRG	0.347	0.896	0.786
GFG	0.405	0.904	0.829

5. Cascade ANN Modelling

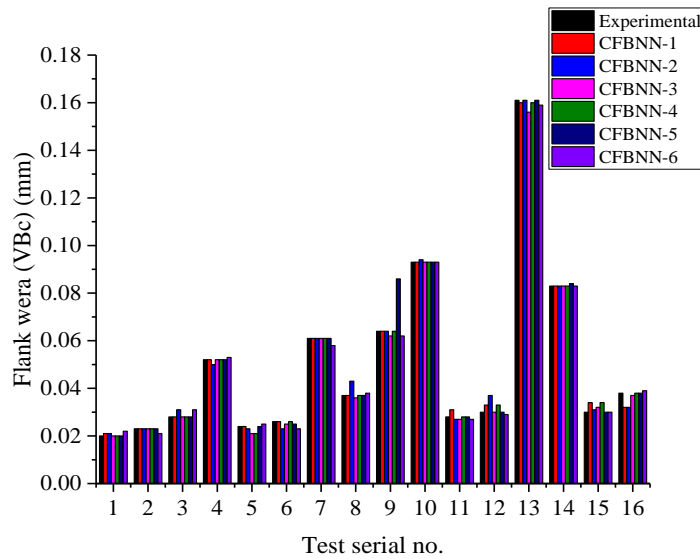
Cascade-forward-back propagation neural network (CFBNN) is a special version of feed-forward neural network (FFNN) but it comprises a connection from the input and each earlier layer to subsequent layers. Similar as FFNN, this network has three distinguish layer such as input layer (each neuron representing the individual input terms, here, number of neurons = number of inputs = n), hidden layer (depends on selected functions rule which is based on 'n') and output layer (representing single output term). In this technique, additional connections like each input to the output layer attributed a faster learning speed with the desired relationship. Also, this technique exhibited the non-linear connection between input and output without eradicating the linear connection among the two [52–53].

The input layer consists of three neurons ($n = 3$) like depth of cut (t), feed (s) and cutting speed (V_c), the output layer consists of one neuron which represents the flank wear (VBc) or chip reduction coefficient (CRC). The hidden layer consists of different numbers of neurons. Zhang et al. [54] proposed that the number of neurons in the hidden layer depends on the number of inputs (n). Number of neurons in hidden layer be taken as $n/2$, n, 2n, n+1, n+2, 2n+1, 2n+2 etc. However, in the current modelling work, six different models based on six different numbers of neurons ($n=3$; $n+1 = 4$; $n+2 =5$, $2n =6$, $2n+1 =7$ and $2n+2 =8$) in hidden layers are utilized. The notation of all six models are as follows: CFBNN-1 (contains 3 neurons in hidden layer), CFBNN-2 (contains 4 neurons in hidden layer), CFBNN-3 (contains 5 neurons in hidden layer), CFBNN-4 (contains 6 neurons in hidden layer), CFBNN-5 (contains 7 neurons in hidden layer) and CFBNN-6 (contains 8 neurons in hidden layer). The schematic representation of the CFBNN model is displayed in Fig. 13. Further, R-square and mean absolute percentage error (MAE) between predicted and experimental data of each output, is estimated and compared. MAE is estimated using Eq. 1.

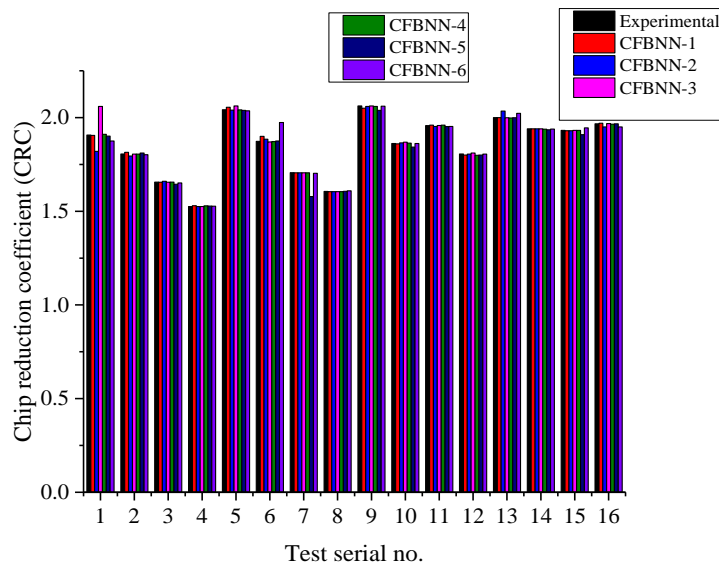
**Fig. 13 - Cascade-forward-back propagation neural network (CFBNN)**

The current work utilized MATLAB R2013a 'nntool' box to establish CFBNN modelling. For this, several functions like 'divderand' for picking random distribution of data, 'trainlm' for training the required data 'learnngdm' for learning, 'mse' for checking the error or performance. For training the data, epochs number, training rate, and gradient are taken as 1000, 0.1 and $1.00e^{-07}$ respectively [55]. Training of the developed network was repeated until achieve the minimum gradient level of validation. Further 'simulation' function is utilized to get the output predicted data. A comparative graph is plotted between experimental and predicted data for all types of models and displayed in Fig. 14. Figure 14 ensured that the predicted results for VBc and CRC are very close to experimental data for all types of CFBNN. Further, from MAE value (Table 10), CFBNN-4 exhibited the lowest mean absolute error for VBC (2.278 %) and CRC (0.112 %) among all types of models. Also from Table 10, the R-square value for all types of models is close to unity but model CFBNN-4 has the highest R-square (for VBc = 0.9988 and for CRC = 0.9997) among all types

of models. As CFBNN-4 type of model is topmost fitted model thus it is recommended to use this model for other modelling works.

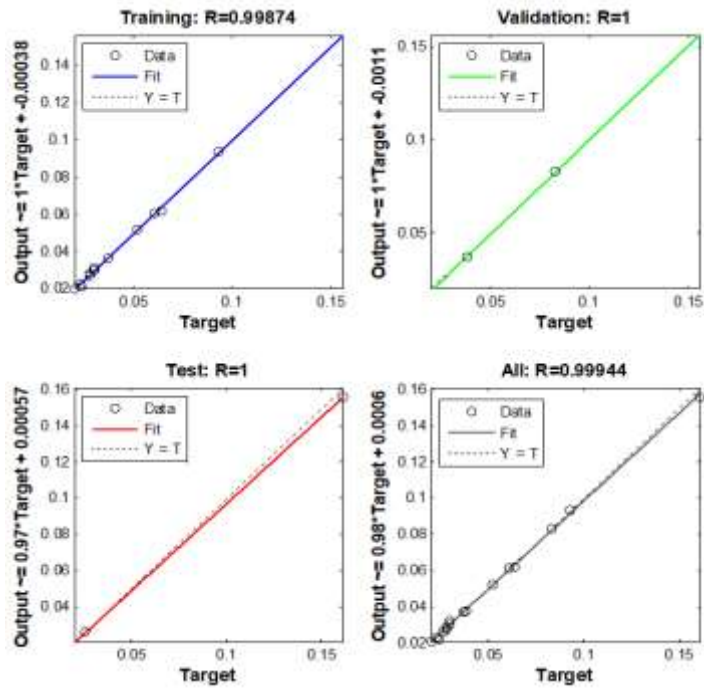


(a)

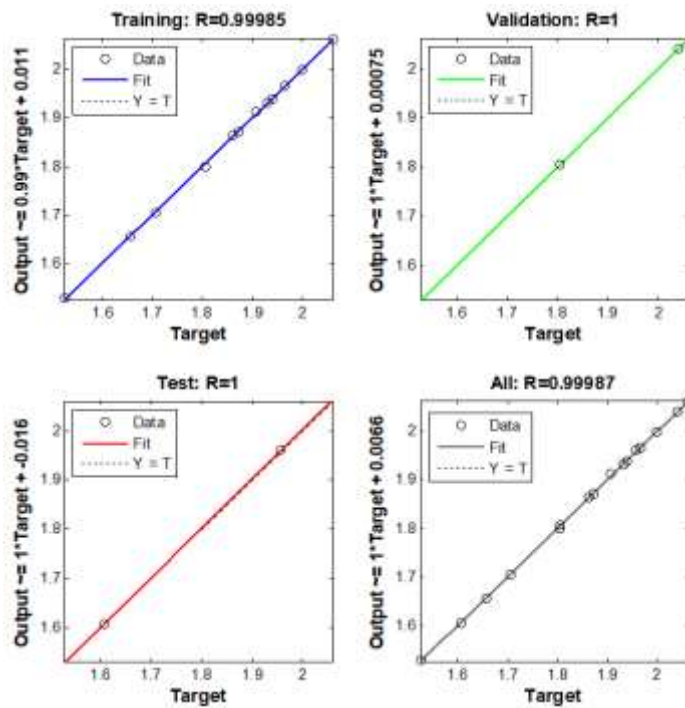


(b)

Fig. 14 - Comparative plot of experimental Vs different CFBNN modelling data (a) Vbc (b) CRC



(a)



(b)

Fig. 15 - Regression graph for Type CFBNN-4 (a) VbC (b) CRC

Table 10 - Estimated values of MAE and R-Square

Model type	Flank wear (VBc)		Chip reduction coefficient (CRC)	
	MAE (%)	R-Square	MAE (%)	R-Square
CFBNN-1 (n=3)	3.466	0.9969	0.289	0.9994
CFBNN-2 (n=4)	6.161	0.9932	0.594	0.9758
CFBNN-3 (n=5)	2.384	0.9985	0.638	0.9494
CFBNN-4 (n=6)	2.278	0.9988	0.112	0.9997
CFBNN-5 (n=7)	2.464	0.9800	0.843	0.9646
CFBNN-6 (n=8)	4.285	0.9979	0.714	0.9689

6. Conclusion and Future Work

Current work focused on the selection of optimal input conditions for dry hard turning using a Grey-fuzzy hybrid optimization concept. Two different types of grey-fuzzy systems were used considering the Gaussian membership function. Flank wear and chip reduction coefficients, and chip morphology were considered as performance criteria. The following major findings are reported as follows:

- Abrasion, micro-chipping, chipping, sever chipping (tool-tip lost) and built-up edge is the wear mechanism identified on to the tool-tip. ANOVA study reported that the impact of cutting speed on VBc was topmost (54.06 %) followed by the depth of cut (26.04 %).
- According to ANOVA, the impact of feed (43.11 %) on CRC is about 2.54 times more than cutting speed (15.92%). Helical (continuous) and broken chips (c and e type) with a saw-tooth pattern are noticed in the entire research study. Majorly higher feed rates are more responsible to get broken chips.
- The mean absolute error between GRG and Type I-GFG is estimated as 4.731% while it is 4.016% for GRG and Type II-GFG. i.e. Type II GFG contains 15 % less error compared to Type I, hence Type II GFG data has been taken to estimate the optimal solution.
- The optimal combination of input terms is found as t-1 (0.15 mm), s-4 (0.25 mm/rev) and v_c-2 (100 m/min) which is comparable to the results obtained under spray impingement cooling in the literature. Running confirmatory experiment results are obtained at the optimal conditions and found an effective improvement in GFG relative to GRG.
- The cascade-forward-back propagation neural network (CFBNN) modelling exhibited a better result with maximum mean absolute error lie under 6.2% for flank wear (VBc) and 1% for the chip reduction coefficient (CRC). CFBNN-4 model exhibited the best prediction results with a mean absolute error of 2.278% for flank wear (VBc) and 0.112% for chip reduction coefficient (CRC). Therefore, CFBNN-4 model is recommended to use this model for other modelling works.

The current work results can be effectively utilized in the industry in a dry environment which can completely eliminate the extra tooling cost as well as environmental issues thus supporting the concept of green manufacturing. In the future, the PVD TiAlN tool can be implemented for higher workpiece hardness (> 55 HRC) to judge the machinability capability. In the future work, some other hybrid approaches such as GA-PSO, ANN-PSO, and ANFIS-PSO can be utilized for the modelling and simulation of AISI D2 Steel.

Acknowledgement

The authors are heartily thankful to the KIIT Deemed to be University, Bhubaneswar to allow us to use their research facilities to complete the current research work.

References

- [1] Patel G. C. M., Chate, G. R., Parappagoudar, M. B., & Gupta, K. (2020). Machining of hard materials. A Comprehensive Approach to Experimentation, Modeling and Optimization. Springer Briefs in Applied Sciences and Technology, doi: 10.1007/978-3-030-40102-3
- [2] Patel G. C. M., Chate, G. R., Parappagoudar, M. B., & Gupta, K. (2020). Machining of hard materials. A Comprehensive Approach to Experimentation, Modeling and Optimization. Springer Briefs in Applied Sciences and Technology, doi: 10.1007/978-3-030-40102-3
- [3] Shnfir, M., Olufayo, O. A., Jomaa, W. & Songmene, V. (2019). Machinability Study of Hardened 1045 Steel When Milling with Ceramic Cutting Inserts. Materials, (12), 3974; doi:10.3390/ma12233974
- [4] Kumar, R., Sahoo, A. K., Mishra, P. C., Das, R. K. & Ukamanal, M. (2018). Experimental investigation on hard turning using mixed ceramic insert under accelerated cooling environment. International Journal of Industrial Engineering Computations, 9, 509–522
- [5] Kumar, R., Sahoo, A. K., Mishra, P. C. & Das R. K. (2018). An investigation to study the wear characteristics and comparative performance of cutting inserts during hard turning. International Journal of Machining and

- Machinability of Materials, 20 (4), 320-344
- [6] Kumar, R., Sahoo, A. K., Mishra, P. C., & Das, R. K. (2018). Comparative investigation towards machinability improvement in hard turning using coated and uncoated carbide inserts: part I experimental investigation. *Advances in Manufacturing*, 6 (1), 52–70
- [7] Qian, L., & Hossan, M. R. (2007). Effect on cutting force in turning hardened tool steels with cubic boron nitride inserts. *Journal of Materials Processing Technology*, 191 (1–3), 274–278
- [8] Shalaby, M. A., El Hakim, M. A., Abdelhameed, M. M., Krzanowski, J. E., Veldhuis, S. C., & Dosbaeva, G.K. (2014). Wear mechanisms of several cutting tool materials in hard turning of high carbon–chromium tool steel. *Tribology International*, (70), 148–154
- [9] Dosbaeva, G. K., El Hakim, M. A., Shalaby, M. A., Krzanowski, J. E., & Veldhuis, S.C. (2015). Cutting temperature effect on PCBN and CVD coated carbide tools in hard turning of D2 tool steel. *International Journal of Refractory Metals and Hard Materials*, 50, 1–8
- [10] Kishawy, H. A. (2002). An experimental evaluation of cutting temperatures during high speed machining of hardened D2 tool steel. *Machining Science and Technology*, 6(1), 67–79
- [11] Arsecularatne, J. A., Zhang, L. C., Montross, C., & Mathew, P. (2006). On machining of hardened AISI D2 steel with PCBN tools. *Journal of Materials Processing Technology*, 171 (2), 244–252
- [12] Salem, S. B., Bayraktar, E., Boujelbene, M. & Katundi, D. (2012). Effect of cutting parameters on chip formation in orthogonal cutting. *Journal of Achievements in Materials and Manufacturing Engineering*, 50(1), 7–17
- [13] Yuan, J., Fox-Rabinovich, G. S., & Veldhuis, S. C. (2018). Control of tribofilm formation in dry machining of hardened AISI D2 steel by tuning the cutting speed. *Wear*, 402–403, 30–37
- [14] Davim, J. P., & Figueira, L. (2007). Machinability evaluation in hard turning of cold work tool steel (D2) with ceramic tools using statistical techniques. *Materials and Design*, 28 (4), 1186–1191
- [15] Davim, J. P., & Figueira, L. (2007). Machinability evaluation in hard turning of cold work tool steel (D2) with ceramic tools using statistical techniques. *Materials and Design*, 28 (4), 1186–1191
- [16] Bartarya, G., & Choudhury S. K. (2012). Effect of cutting parameters on cutting force and surface roughness during finish hard turning AISI52100 grade steel. *Procedia CIRP*, 1, 651–656
- [17] Bartarya, G. & Choudhury, S. K. (2013). Influence of machining parameters on forces and surface roughness during finish hard turning of EN 31 steel. *Proceeding Institution of Mechanical Engineering Part B: Journal of Engineering Manufacture*, 228 (9), 1068–1080
- [18] Zeghni, A. E., & Hashmi, M. S. J. (2004). Comparative wear characteristics of TiN and TiC coated and uncoated tool steel. *Journal of Materials Processing Technology*, 155–156, 1923–1926
- [19] Haron, C. H. C., Ginting, A., & Goh, J. H. (2001). Wear of coated and uncoated carbides in turning tool steel. *Journal of Materials Processing Technology*, 116 (1–3) 49–54
- [20] Chinchankar, S., & Choudhury, S. K. (2014). Evaluation of chip-tool interface temperature: effect of tool coating and cutting parameters during turning hardened AISI 4340 steel. *Procedia Materials Science*, (6), 996–1005
- [21] Chinchankar, S., & Choudhury, S. K. (2014). Characteristics of wear, force and their interrelationship: In process monitoring of toll within different phases of the tool life. *Procedia Materials Science*, (5), 1424–43.
- [22] Panda, A., Das, S. R., & Dhupal, D. (2020). Machinability investigation and sustainability assessment in FDHT with coated ceramic tool. *Steel and Composite Structures*, 34(5), 681-698
- [23] Panda, A., Ranjan Das, S., & Dhupal, D. (2019). Machinability Investigation of HSLA Steel in Hard Turning with Coated Ceramic Tool: Assessment, Modeling, Optimization and Economic Aspects. *Journal of Advanced Manufacturing Systems*, 18(04), 625-655
- [24] Das, A., Tirkey, N., Patel, S. K., Das, S. R., & Biswal, B. B. (2019). A comparison of machinability in hard turning of EN-24 alloy steel under mist cooled and dry cutting environments with a coated cermet tool. *Journal of Failure Analysis and Prevention*, 19(1), 115-130
- [25] Das, A., Patel, S. K., Biswal, B. B., & Das, S. R. (2019). Machinability investigation and cost estimation during finish dry hard turning of AISI 4340 steel with untreated and cryo treated cermet inserts. *Journal of Superhard Materials*, 41(4), 247-264
- [26] Anand, A., Behera, A. K., & Das, S. R. (2019). An overview on economic machining of hardened steels by hard turning and its process variables. *Manufacturing Review*, 6, 4
- [27] Senthilkumar, N., Sudha, J. & Muthukumar, V. (2015). A grey-fuzzy approach for optimizing machining parameters, and the approach angle in turning AISI 1045 steel. *Advances in Production Engineering & Management*, 10(4), 195–208
- [28] Horng, J-T., & Chiang, K-T. (2008). A grey and fuzzy algorithms integrated approach to the optimization of turning Hadfield steel with Al₂O₃/TiC mixed ceramic tool. *Journal of Materials Processing Technology*, 207, 89–97
- [29] Suresh, P., Marimuthu, K., Ranganathan, S., & Rajmohan, T. (2014). Optimization of machining parameters in turning of Al–SiC–Gr hybrid metal matrix composites using grey-fuzzy algorithm, *Transactions of Nonferrous*

- Metals Society of China, 24, 2805–2814
- [30] Krishnamoorthy, A., Boopathy, S. R., Palanikumar, K., & Davim, J. P. (2012). Application of grey fuzzy logic for the optimization of drilling parameters for CFRP composites with multiple performance characteristics. *Measurement*, 45, 1286–1296
- [31] Das, B., Roy, S., Rai, R. N., & Saha, S.C. (2016). Application of grey fuzzy logic for the optimization of CNC milling parameters for Al–4.5%Cu–TiC MMCs with multi-performance characteristics. *Journal of Engineering Science and Technology*, 19, 857–865
- [32] Kumar, R., Sahoo, A. K., Das, R. K., Panda, A., & Mishra, P. C. (2018). Modelling of flank wear, surface roughness and cutting temperature in sustainable hard turning of AISI D2 steel. *Procedia Manufacturing*, 20, 406-413
- [33] Panda, A., Sahoo, A., & Rout, A. (2017). Statistical regression modeling and machinability study of hardened AISI 52100 steel using cemented carbide insert. *International Journal of Industrial Engineering Computations*, 8(1), 33-44
- [34] Özbek, O., & Saruhan, H. (2020). The effect of vibration and cutting zone temperature on surface roughness and tool wear in eco-friendly MQL turning of AISI D2. *Journal of Materials Research and Technology*
- [35] Bartarya, G., & Choudhury, S. K. (2012). State of the art in hard turning. *International Journal of Machine Tools and Manufacture*, 53(1), 1-14
- [36] Panda, A., Sahoo, A. K. & Rout, A. K. (2016). Multi-attribute decision making parametric optimization and modeling in hard turning using ceramic insert through grey relational analysis: A case study. *Decision Science Letters*, (5), 581–592
- [37] Kumar, R., Sahoo, A. K., Mishra, P. C., and Das R. K. (2019). Measurement and machinability study under environmentally conscious spray impingement cooling assisted machining. *Measurement*, 135, 913–927
- [38] Sahoo, P., Satpathy, M. P., Singh, V. K., & Bandyopadhyay, A. (2018). Performance evaluation in CNC turning of AA6063-T6 alloy using WASPAS approach. *World Journal of Engineering*, 15(6), 700–709
- [39] Dong, P. Q., Duc, T. M., Tuan, N. M., Thanh, D. V., & Truong, N. V. (2020). Improvement in the Hard Milling of AISI D2 Steel under the MQCL Condition Using Emulsion-Dispersed MoS₂ Nanosheets. *Lubricants*, 8(6), 62
- [40] Kumar, R., Sahoo, A. K., Mishra, P. C., & Das R. K. (2020). Influence of Al₂O₃ and TiO₂ nanofluid on hard turning performance. *International Journal of Advanced Manufacturing Technology*, 106, 2265-2280
- [41] Singh, B. K., Roy, H., Mondal, B., Roy, S. S., & Mandal, N. (2019). Measurement of chip morphology and multi criteria optimization of turning parameters for machining of AISI 4340 steel using Y-ZTA cutting insert. *Measurement*, 142, 181-194
- [42] Kumar, R., Choudhury, A. R., Sahoo, A. K., Panda, A., & Malakar, A. (2020). Machinability Investigation on Novel Incoloy 330 Super Alloy using Coconut Oil Based SiO₂ Nano fluid. *International Journal of Integrated Engineering*, 12(4), 145-160
- [43] Kumar, R., Sahoo, A. K., Mishra, P. C., & Das R. K. (2019). Investigation on Tool Wear and Surface Characteristics in Hard Turning under Air-Water Jet Spray Impingement Cooling Environment. *Tribology in Industry*, 41(2), 172–187
- [45] Palanisamy, D., & Senthil, P. (2018). Application of grey-fuzzy approach for optimization of CNC turning process. *Materials Today: Proceedings*, 5, 6645–6654
- [46] Xu, G., Guo, P., Li, X., & Jia, Y. (2014). Grey relational analysis and its application based on the angle perspective in time series. *Journal of Applied Mathematics*, Volume 2014, Article ID 312645, 1-10, <https://doi.org/10.1155/2014/312645>
- [47] Palanikumar, K., Karunamoorthy, L., & Karthikeyan, R. (2006). Multiple performance optimization of machining parameters on the machining of GFRP composites using carbide (K10) tool. *Journal of Materials and Manufacturing Processes*, 21, 846–852
- [48] Pattnaik, S., Karunakar, D.B., Jha, P.K. (2013). Multi-characteristic optimization of wax patterns in the investment casting process using grey-fuzzy logic. *International Journal of Advanced Manufacturing Technology*, 67(5–8), 1577–1587
- [49] Zainudin, A., Sia, C. K., Ong, P., Narong, O. L. C., Azlan, M. A., & Lee, W. K. (2019). Performance properties optimization of triaxial ceramic-palm oil fuel ash by employing taguchi grey relational analysis. *International Journal of Integrated Engineering*, 11(1), 257-269
- [50] Soepangkat, B. O. P., Norcahyo, R., Pramujati, B., & Wahid, M.A. (2019). Multi-objective optimization in face milling process with cryogenic cooling using grey fuzzy analysis and BPNN-GA methods. *Engineering Computations*, 36(5), 1542–1565
- [51] Kumar, R., Sahoo, A. K., Mishra, P. C., & Das, R. K. (2019). Performance assessment of air-water and TiO₂ nanofluid mist spray cooling during turning hardened AISI D2 steel. *Indian Journal of Engineering and Materials Sciences*, 26, 235-253
- [52] Goyal, S., & Gyandera, G. K. (2011). Cascade and feedforward backpropagation artificial neural network models for prediction of sensory quality of instant coffee flavoured sterilized drink, *Canadian Journal on Artificial Intelligence. Machine Learning and Pattern Recognition*, 2(6), 78-82

- [53] Warsito, W., Santoso, R., Suparti, & Yasin, H. (2018). Cascade Forward Neural Network for Time Series Prediction. IOP Conf. Series: Journal of Physics: Conference Series, 1025, 012097
- [54] Zhang, G., Patuwo, B. E., & Hu, M. Y. (1998). Forecasting with artificial neural networks: The state of the art. International Journal of Forecasting, 14, 35–62
- [55] Idrus, M. N. E. M., Chia, K. S., Sim, H. M., Al-kaf, H. A. G. (2018). Artificial neural network and savitzky golay derivative in predicting blood hemoglobin using near-infrared spectrum, International Journal of Integrated Engineering, 10(8), 112-119